J. Fluid Mech. (1980), *vol.* 98, *part* 1, *pp.* 49–63
Printed in Great Britain

Observations and LDA† measurements of confined turbulent vortex flow

By M. P. ESCUDIER, J. BORNSTEIN AND N. ZEHNDER

Brown Boveri Research Centre, CH-5405 Baden-Dättwil, Switzerland

(Received 6 June 1979)

A series of LDA measurements and visual observations of confined turbulent vortex flow are described. The experiments were performed with water as the fluid medium in a vortex tube of length-to-diameter ratio $L/D = 3{\cdot}8$ for a range of exit diameters D_e between $D_e/D = 1$ and $0{\cdot}18$. The experiments reveal a remarkable change in the vortex structure as D_e is reduced: from a thick core with an axial-velocity defect in the centre, and even reversed flow, to a thin annular jet-like core with a peak axial velocity more than an order of magnitude greater than the average value and again a central velocity deficit. The corresponding swirl profiles are not remarkable and are well-represented under all conditions by the solution of Burgers (1948), albeit with a velocity maximum which is strongly dependent upon D_e.

1. Introduction

The cyclone separator, vortex whistle, fluidic vortex valve, Ranque–Hilsch tube, swirl combustor and gas-core nuclear rocket are among numerous practical devices the performance of which is dominated by a confined turbulent vortex created by tangential injection of all or part of the through-flow. The present authors' interest in confined-vortex flow is motivated by its importance with regard to the characteristics of the inlet and outlet chambers of conventional axial-flow turbomachines where, in contrast to the other applications mentioned, the presence of a vortex is largely fortuitous and leads to such undesirable characteristics as periodic flow oscillations and a circumferentially non-uniform distribution of pressure (Escudier & Merkli 1979; Merkli & Escudier 1979), as well as high pressure loss (Escudier 1979).

The complex nature and technical significance of vortex flows has led not unnaturally to an extensive literature on the subject: the review of Lewellen (1971), for example, lists more than 400 references. Conspicuously lacking, however, have been detailed measurements of vortex structure, even in idealized laboratory experiments, the problem being that vortex flows are extremely sensitive to disturbances created by even the smallest probes (e.g. Holman & Moore 1961). Intrusive measurements are therefore of questionable value, and reliable experimental observations have been largely limited to surface pressure measurements and flow visualization. This situation is now changing thanks to the development of the LDA technique which permits complete mapping of vortex and other probe-sensitive flows. At least two such confined-vortex studies have been published in recent years, the first by Orloff & Bossel

† Laser-Doppler anemometer.

0022-1120/80/4441-8940 $02.00

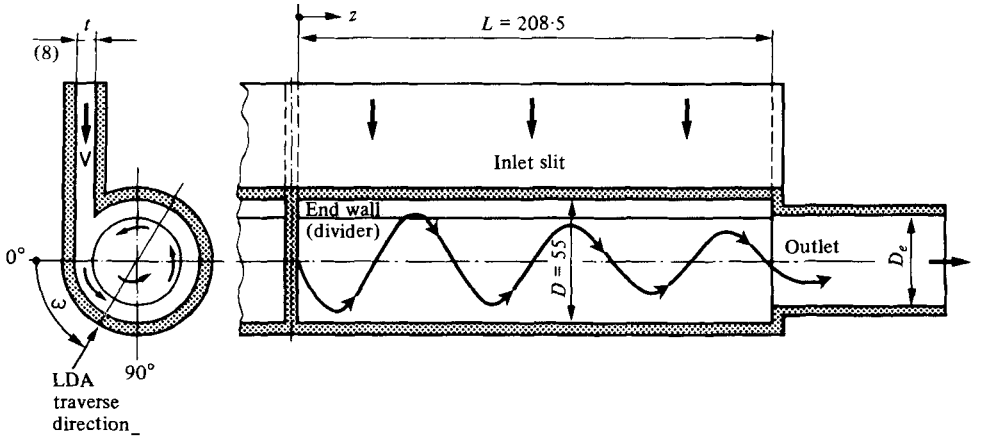

FIGURE 1. Schematic diagram of the vortex tube (linear dimensions in mm).

(1973) and the second by Faler & Leibovich (1977) based upon the thesis of Faler (1976) both primarily concerned with vortex breakdown. The probe-interference problem has also led to the use of the LDA to measure velocity distributions in trailing vortices with results being reported, for example, by Orloff (1974) and Baker *et al.* (1974).

In this paper we present LDA measurements, supported by flow visualization, of the mean axial- and swirl-velocity distributions for flow in a straight, jet-driven, vortex tube with the inlet slit running along its entire length (figure 1). The geometry of this model was developed from the ring-tube exit-chamber geometry, discussed in the recent paper by Escudier & Merkli (1979), in which some preliminary LDA measurements were made but which were discontinued in favour of the present investigation in view of the additional complexity of the flow in the ring, engendered in large part by Coriolis forces arising as a result of the toroidal geometry. Our vortex-tube geometry is also close to that envisaged by N.A.S.A. some years ago for a gas-cored nuclear rocket, although for that application the flow entered through multiple symmetrically-situated slits. Besides being appropriate for our exit-chamber configuration, the presence of a single slit simplifies considerably the problem of optical access which is critical for application of the LDA. At the same time, as will be seen, it is unfortunately the case that this arrangement apparently leads to some distortion of the vortex.

The theoretical analysis of vortex flows is extremely difficult, and relatively little progress has been made, although the similarity solutions for laminar flow calculated by Donaldson & Sullivan (1960) provide useful insight into the nature of vortex flow. The special case of uniform axial velocity $w = \alpha z$, α being a constant, was actually first analysed by Burgers (1948) and leads to the simple result for the swirl distribution

$$v = \frac{\Gamma}{2\pi r}[1 - e^{\alpha r^2/4\epsilon}],$$

where Γ is the circulation and ϵ the eddy viscosity.

This expression has been used by Faler & Leibovich (1978) and others as a basis of comparison for swirl-velocity measurements, and will also be adopted for the same purpose in the present paper whilst recognizing that (as the measurements clearly show) the axial velocity distribution is in fact generally far from uniform. Also in most

practical situations, the vortex core is turbulent and so an eddy viscosity ϵ has been substituted for the kinematic viscosity ν in the above formula.

The term vortex core is taken here to mean the central viscous or turbulent region of the vortex, characterized by a closely-linear variation of the swirl velocity (i.e. $v \sim r$). The radial position at any axial location where $v = 0$ is then the centre of the vortex and the radial distance between the positive and negative swirl maxima is used as a quantitative measure of the core diameter. It became clear during the course of the investigation that the vortex core was not concentric with the tube axis and so the radial-position variable r (measured from the vortex centre) is not in general identical with the radial distance from the tube centre r'.

Although this report is primarily concerned with turbulent vortex flow, some results of flow visualization at low Reynolds numbers, where the flow is either laminar or not fully turbulent, are presented briefly.

2. Flow apparatus and measuring equipment

The vortex tube shown schematically in figure 1 forms part of a gravity-fed water circuit in which the through-flow can be dumped or recirculated. The mass flow rate is normally determined by measuring the pressure difference across a venturi built into a straight section of the supply tube connecting the upper tank of the water circuit and the header which feeds the inlet slit of the vortex tube. Very low flow rates (up to about $0{\cdot}25\ \mathrm{l\,s^{-1}}$) were more accurately measured from the time required to fill a container of known volume. The maximum attainable flow rate through the vortex tube varies with the geometric configuration, and may be reduced by a gate valve on the downstream side of the tube.

Since it was felt that dimensional fidelity could not be maintained if the longitudinal inlet slit were cut in a simple round tube, the vortex tube was machined from solid Plexiglas with sufficient accuracy to permit measurements using a backscatter LDA system. The wall thickness of the tube is 5 mm, the inside diameter $D = 55$ mm and the overall length is 425 mm. The tube is so constructed that the inlet-slit width t can be changed through the use of inserts, the exit diameter D_e altered using 83 mm long cylindrical outlet sections which may be inserted in the tube ends, both of which are open. The open lengths of the tube are varied by the installation at various axial locations of a divider comprising a splitter plate in the inlet slit combined with a circular disk in the tube itself. It is also possible to close off one end of the tube completely and/or to omit the divider. For most of the LDA measurements reported here, $t = 8$ mm and the divider was installed half way along the tube thereby dividing it into two equal lengths with $L = 208{\cdot}5$ mm (the difference of 8 mm between $2L$ and the tube length corresponds to the thickness of the divider) corresponding to a ratio $L/D = 3{\cdot}8$. The possibility of carrying out experiments with both ends of the tube open and no divider offers in principle the advantage of making measurements in a flow free from the effects of the end-wall boundary layer which develops on the disk. Although in practice difficulties were experienced with this set-up with regard to flow symmetry, a few such experiments have been carried out to date and are reported here for purposes of comparison. This symmetry problem was also encountered by Binnie & Teare (1956).

Of principal interest in the present series of measurements was the influence on the

vortex structure of the exit diameter. With the divider installed, for D_e = 55, 40, 25, 18 and 10 mm, swirl- and axial-velocity distributions have been measured at the axial locations z = 8·5, 38·5, 78·5, 118·5, 158·5 and 198·5 mm, with additional measurements at z = 198·5 mm for D_e = 15, 17·5, 19, 20 and 22·5 mm. In the absence of the divider, axial-velocity distributions have been measured at z = 193·5 mm for D_e = 55, 40, 25 and 10 mm.

For the two largest exits, the volumetric flow rate Q† was set at about 1·0 l s^{-1}, LDA measurements at higher flow rates being precluded by the onset of gaseous cavitation within the low-pressure vortex core. The corresponding Reynolds number

$$Re\,(\equiv Vt/\nu) = 4800.$$

For the smaller exits, however, cavitation occurred at even lower flow rates and was avoided by running the experiment with Q = 0·4 l s^{-1} (Re = 1900). Check measurements of velocity distributions with Q = 0·4 l s^{-1} for D_e = 40 and 55 mm showed only a scale difference appropriate to the reduced mass flow.

To define a swirl parameter we require some measure of the ratio of angular to axial momentum, with $\Omega \equiv \Gamma D_e/Q$ being a suitable choice. Taking the circulation $\Gamma = \pi DV$, where V is the velocity in the inlet slit, gives $\Omega = \pi DD_e/Lt$, since $Q = VLt$. For D_e in the range 10 to 55 mm, we therefore have Ω varying from 1·0 to 5·7.

The LDA system used is a prototype of the BBC–Goerz dual-beam back-scatter instrument employing a 5 mW He–Ne laser and incorporating a Bragg cell after the beam splitter to shift the frequency of one beam by 40 MHz, so permitting the determination of both the magnitude and direction of the velocity component being measured. The focal length of the focussing lens is 115 mm which, combined with a beam separation of 25 mm, produces a half angle of 6·2° between the two beams and a measuring control volume approximately 2 mm in length, though the effective length is reduced appreciably by appropriate selection of the threshold level for the signal-processing electronics. Although it is realized that in regions of high curvature of the velocity distribution the spatial resolution is therefore inadequate, there is little doubt regarding the qualitative trends of the data and even, for the most part, the quantitative results. A correction lens was designed and machined from Plexiglas to correct for the cylindrical aberration introduced by the curved wall of the vortex tube. All measurements were made in de-ionized water seeded with 5·7 μm Dow latex spheres, these producing Doppler signals of relatively high signal-to-noise ratio.

Traverses can be made across practically any diametral plane since the tube, inlet slit and header assembly can be rotated by more than 180° about the tube axis. As is discussed below, this possibility of rotating the model proved extremely valuable in determining the precise location of the vortex core. Measurements were made with the LDA optical head mounted on a three-degrees-of-freedom traverse, the head being stepped forward in 0·5 mm increments (0·7 mm within the model). Doppler frequencies were determined from the output voltage of the photomultiplier tube using a sampling spectrum analyser system with an overall bandwidth of 30 kHz. The basic processing electronics used is described by Iten & Dändliker (1972). A PDP 11/05 mini-computer was used both to control the traverse and also to store and preprocess the flow parameters, Doppler frequencies and position information. For both the swirl- and axial-

† Q refers to the flow rate through one of the two outlets.

velocity components, 100 discrete measurements were made at each location and the average values and standard deviation σ computed. Values falling outside $\pm 2{\cdot}8\sigma$ of the means were discarded (Chauvenet's criterion) and additional data acquired until 100 acceptable points had been accumulated. At certain locations reflexions from solid boundaries produced spurious values for the swirl component which nevertheless satisfied this criterion; these data were subsequently discarded.

For practical reasons, the experimental set up used for flow visualization was different from that for the LDA measurements having only a single outlet but with an equivalent 'wetted' geometry. To mark the fluid, water-soluble dyes were injected into the flow through 1 mm diameter surface holes at various locations. At high flow rates cavitation of the vortex core also provided a means of visualizing the flow. For the camera set up employed, radial distances appear about 25 % too large owing to refraction at the outer surface of the tube.

3. Flow visualization

The series of photographs for $D_e = 25$ mm in figure 2 (plate 1) illustrates the transition from laminar to turbulent flow and subsequently to a hollow cavitated core. The closed end of the vortex tube is to the left and the entrance to the outlet contraction is seen as a slender vertical ellipse to the right. The red dye is injected into the flow through a hole in the centre of the end wall and the blue dye through a hole offset radially by 18 mm. The green dye (figure 2*a* only) is introduced into the flow in the inlet slit. Except for a progressively pronounced axial thinning of the coloured core zone as D_e is reduced, and the absence of cavitation for $D_e = 10$ mm, these photographs for $D_e = 25$ mm are also typical of those for obtained $D_e = 18$ mm and 10 mm.

In figure 2(*a*), which is for the lowest flow rate $Q = 0{\cdot}014\ \mathrm{l\,s^{-1}}$, corresponding to a Reynolds number $Re\,(\equiv Vt/\nu) = 64$, the flow is laminar and shows no sign of the distinct core structure which is evident in the subsequent photographs for higher flow rates. At this low flow rate the red dye, which is slightly denser than pure water, tends to sink somewhat before being swept spirally inwards within the end-wall boundary layer. The blue dye, on the other hand, is injected into a region where the external swirl velocity is higher and is swept inwards immediately. The nature of the end-wall boundary layer is presumably similar to that discussed by Bödewadt (1940) for an outer flow of constant angular velocity. Close to the tube centre, both dye streaks peel away from the end wall and then spiral around the vortex centreline towards the tube exit. The green dye also ultimately spirals towards the outlet, after first turning toward the end wall, showing the existence of reversed flow near the tube wall.

The green dye filament as shown in figure 2(*a*) follows a smooth, steady path. In practice, however, difficulty was experienced in achieving this flow state because after a short time, especially when the flow was exposed to heat from the lamps used for illumination, the green dye filament began to fluctuate randomly. This behaviour reveals the marginally stable nature of the outer flow, consistent with Rayleigh's stability criterion for a rotating flow in which the stability decreases with increasing radius towards neutral as (anticipating the structure of the flow) the swirl velocity profile changes from nearly linear to hyperbolic.

As shown by figure 2(*b*), for $Q = 0{\cdot}024\ \mathrm{l\,s^{-1}}$ ($Re \simeq 120$), at this increased flow rate a well defined core structure is already apparent. Strong longitudinal shearing is evident

from the sheath-like appearance of the dyed fluid. It also appeared to the eye that the axial velocity was highest close to the core centre. The green dye, if introduced in the inlet slit, was rapidly diffused, confirming the less stable nature of the outer flow.

With a further increase in flow rate, to $Q = 0{\cdot}040\ \mathrm{l\,s^{-1}}$ ($Re = 190$), as for figure 2(*c*), the laminar core gives way to a quasi-turbulent core in which, again in accordance with Rayleigh's stability criterion, the radial mixing is clearly much less vigorous than the longitudinal and the boundary of the core region is still well defined.

In the next photograph, figure 2(*d*), for $Q = 0{\cdot}10\ \mathrm{l\,s^{-1}}$ ($Re = 480$), an interesting feature of the flow is revealed by the persistence of red dye in the core centre and at its outer edge after switching the red dye supply off. This behaviour suggests an axial velocity variation with regions of slow moving fluid near the vortex centre and at its edge and with higher velocities in between.

The only essential change with an increase in flow rate to $Q = 0{\cdot}40\ \mathrm{l\,s^{-1}}$ ($Re = 1900$), as in figure 2(*e*), is the development of a pronounced bending of the core centre-line. Other features of the core structure remain however: the well-defined edge, suppressed radial mixing in an otherwise fully-turbulent core, and regions of high and low axial velocity similar to those inferred for $Q = 0{\cdot}10\ \mathrm{l\,s^{-1}}$.

The final photograph in this series, figure 2(*f*), for the maximum achievable flow rate $Q = 3{\cdot}2\ \mathrm{l\,s^{-1}}$ ($Re = 15200$), shows the existence of a hollow core produced by gaseous cavitation. An increase in pressure in the outlet tube, partly due to dissipation, allows the vortex core to close again.† The appearance of the hollow core is similar to the helical core shown by Binnie & Teare (1956) for swirling flow through a convergent nozzle.

For $D_e = 40$ and 55 mm, the appearance of the flow below about $0{\cdot}04\ \mathrm{l\,s^{-1}}$ is little different than for the smaller exits. For higher flow rates there are differences, however, as shown by the two series of photographs in figures 3 and 4 (plates 2 and 3).

For $D_e = 40$ mm, the velocity deficit in the core centre is especially pronounced, as may be seen in figure 3(*b*). In fact at a flow rate of $0{\cdot}80\ \mathrm{l\,s^{-1}}$ ($Re = 3800$), figure 3(*d*), the tail of red dye persists long after the supply is cut off and shows sporadic backflow. The core is also much thicker and relatively straight compared with $D_e = 25$ mm.

For $D_e = 55$ mm, the core is even thicker, and the red dye tail again shows the central core to be essentially stagnant. Figure 4(*e*), for the maximum achievable flow rate of $5{\cdot}7\ \mathrm{l\,s^{-1}}$ ($Re = 27000$) shows one stage in the development of the hollow core. Significant changes in the hollow-core structure occur as its diameter changes owing, for example, to the reduction in air content of the water with time or as a result of air injection. Details of these changes are to be found in the paper by Keller & Escudier (1980). A final point which may be observed is that the hollow core, in all cases, is surrounded by a coloured sheath of turbulent fluid extending essentially to the same diameter as would be the case for the filled core at a lower flow rate (e.g. $0{\cdot}8\ \mathrm{l\,s^{-1}}$).

Observations of the flow in the outlet contraction also cast some light on the behaviour of the flow in the main tube itself. The most significant feature to be observed is the occurrence of an axisymmetric bubble form of vortex breakdown, most probably type 0 of Faler & Leibovich (1977). The breakdown appears first at low flow rates downstream of the outlet contraction and then moves upstream into the contraction with increase in the flow rate. Photographs of the breakdown flow within the contrac-

† The response of a hollow core vortex to such an axisymmetric disturbance as the outlet contraction is discussed in detail by Keller & Escudier (1980).

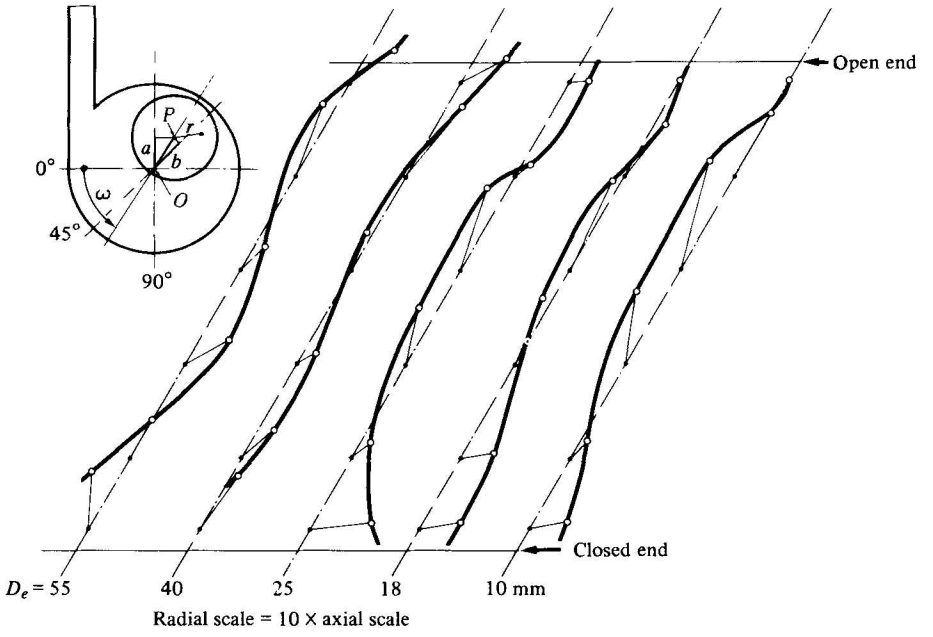

FIGURE 6. Path of the vortex core and (inset) the determination of the core position.

tion are shown in figure 5 (plate 4) for D_e = 18, 25 and 40 mm, the flow rates being 0·34, 0·14 and 0·043 l s^{-1} respectively. A fourth photograph, for D_e = 10 mm, is included although no breakdown could be produced in this case – presumably because the maximum flow rate of 0·67 l s^{-1} is still too low. No photograph is included for D_e = 55 mm, since in this case the flow in the exit section shows no particular structure, and no breakdown is observed. With a further increase in flow rate, the breakdown bubble moves upstream to the contraction inlet. The changes in core structure discussed earlier suggest that the breakdown does not propagate further upstream, although it can no longer be identified as the flow rate is increased. Only when the flow rate is changed rapidly, or shut off completely, does the bubble run into the main tube and collapse.

4. LDA measurements

The non-concentricity of the vortex core and the tube, evident from flow visualization at the higher flow rates where LDA measurements were to be made, indicated that it would be necessary to adjust the measuring angle ω (see figure 1) of the LDA system if a useful representation of the velocity field in the vicinity of the vortex core was to be achieved. As mentioned earlier, the flow system was designed to allow rotation of the entire header–inlet–tube assembly about the tube axis, so that what was necessary was to determine for each measuring set up (i.e. each combination of D_e, z and Q) the appropriate value of ω and rotate the flow model accordingly, the LDA system remaining fixed with its optical axis horizontal and orthogonal to the tube axis. The inset in figure 6 shows how ω and the position of the vortex centre are determined. In each case, coarse (20 point average) preliminary measurements are made of the

apparent swirl-velocity profile $v'(r';\omega)$ in the core region for $\omega = 45°$ and $90°$, yielding two virtual vortex centres (where $v' = 0$) at A and B. Assuming the vortex to be locally axisymmetric, it is a matter of simple trigonometry to show that

$$\cot\omega = \frac{\sqrt{2}b}{a} - 1 \quad \text{and} \quad OP = \frac{a}{\sin\omega}.$$

Although the maximum displacement of the vortex centre OP is only 4·1 mm (for $D_e = 10$ mm), in such an extreme case where the core diameter is only about 2 mm it would be possible to 'miss' the vortex core entirely and such a correction is therefore clearly necessary.

The main part of figure 6 shows schematically the path of the vortex centre for the main range of exit diameters. For clarity the radial scale is 10 × the axial scale, thereby grossly exaggerating the actual core displacement. Several interesting features emerge from these measurements. First, there is a strong dependence on D_e. Near the closed end, for example, ω decreases from 87° for $D_e = 55$ mm to 55° for $D_e = 40$ mm and to about 10° for the smaller exits. A second feature, which is contrary to expectation, is that the core centre does not follow a spiral path with the flow but rather in most cases turns back into the flow towards the exit. Not surprisingly, however, the core is fairly well centred with respect to the tube towards the exit for the smaller diameters.

The principal results of this investigation are represented by the LDA measurements given in figures 7, 8 and 10 of the swirl and axial components of the mean velocity field of the vortex for the flow in the tube with the divider installed. These measurements are clearly consistent with the inferences drawn earlier from flow visualization. The smooth curves drawn through the measured points for the axial velocity have no theoretical significance. Both the axial and swirl profiles show the dominant influence on the flow of the exit contraction. The grey shaded bands in figure 7 represent the extent of the vortex core, as deduced from the swirl profiles. For the two smaller exits, the core defined in this way is significantly narrower than the axial-velocity distributions would suggest. The strong dependence of the core diameter d on D_e is again clear. In addition, figures 7 and 8 show that the entire character of the axial profile within the core changes as the exit diameter is reduced.

For $D_e = 55$ and 40 mm, the core is a region of velocity deficit and even slight reverse flow, behaviour which was to be expected in the light of both previous theoretical and experimental investigations. Thus Nuttall (1953) many years ago reported briefly on a visualization study of swirling tube flow in which flow reversal was observed, and transition to the reversed-flow two-cell solution of Sullivan (1959) was reported in the experimental study of Donaldson & Snedeker (1962) for values of the ratio of a characteristic swirl velocity to a characteristic radial velocity in excess of three. For our experiments, the value of this ratio may be estimated as $\pi D/t \cong 22$, which is clearly greater than the Donaldson–Snedeker criterion. Much more remarkable are the measurements for the smaller exit diameters which reveal a progressive trend to a velocity excess on the vortex core, although Binnie & Teare (1956) concluded that for a hollow-core vortex an axial velocity excess occurs in the thin boundary layer of fluid in solid-body rotation which surrounds the core. Binnie and Teare also observed reversed flow, but in the free vortex zone beyond the core boundary layer. Figure 8, which shows the transition process in detail through a series of axial-velocity profiles measured close to the tube exit ($z = 198{\cdot}5$ mm), reveals that the change in the charac-

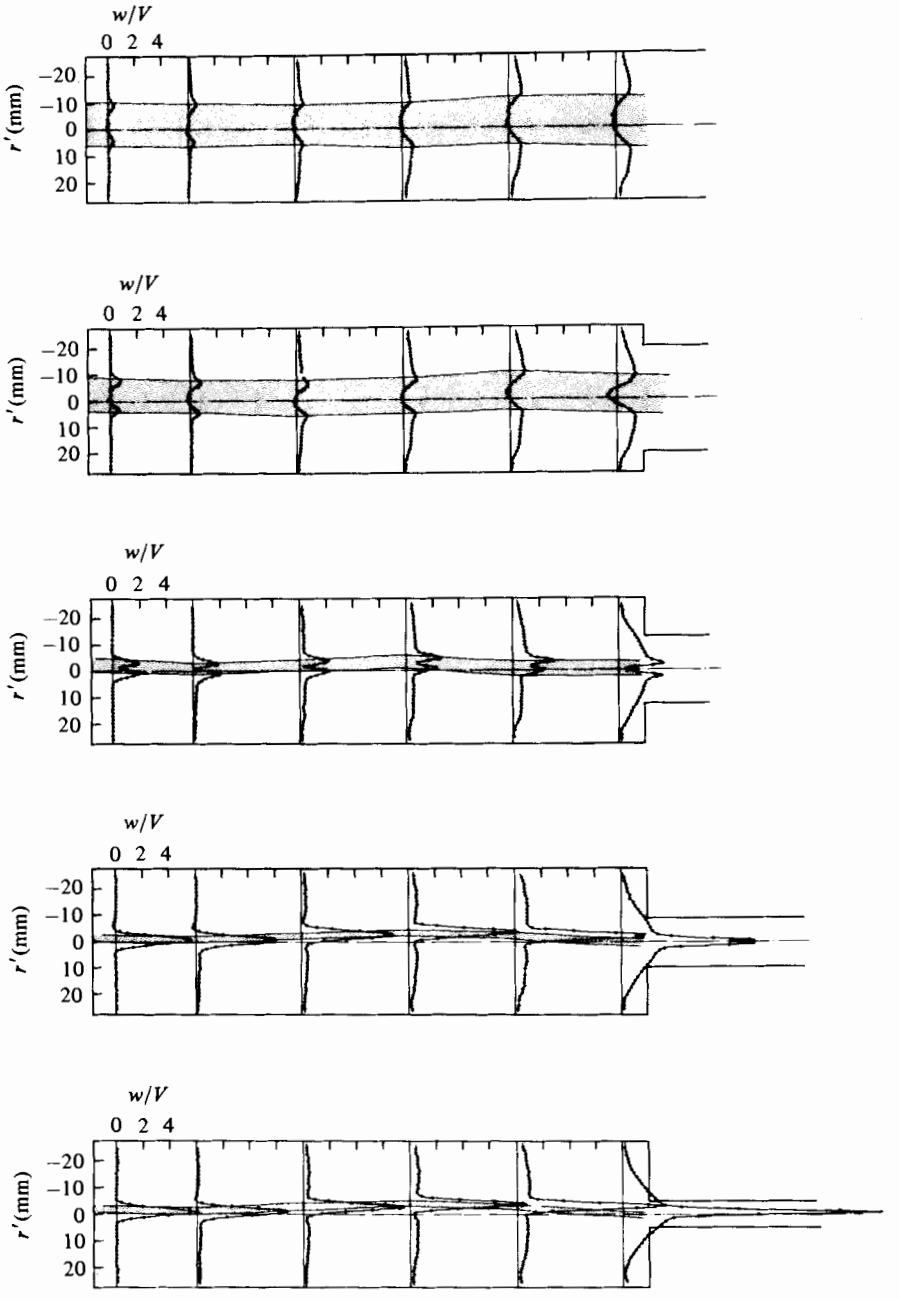

FIGURE 7. Normalized axial-velocity distributions, w/V against r'.

ter of the velocity distribution is progressive rather than sudden. Flow visualization indicates the existence of low velocities in the core centre even for small exits, and it is likely that only the resolution of the LDA instrument prevents this from being seen in the axial velocity profiles. Also included for each profile in figure 8 is a vertical line representing the average axial velocity $w/V \cong 0{\cdot}7$ at this location compared with a

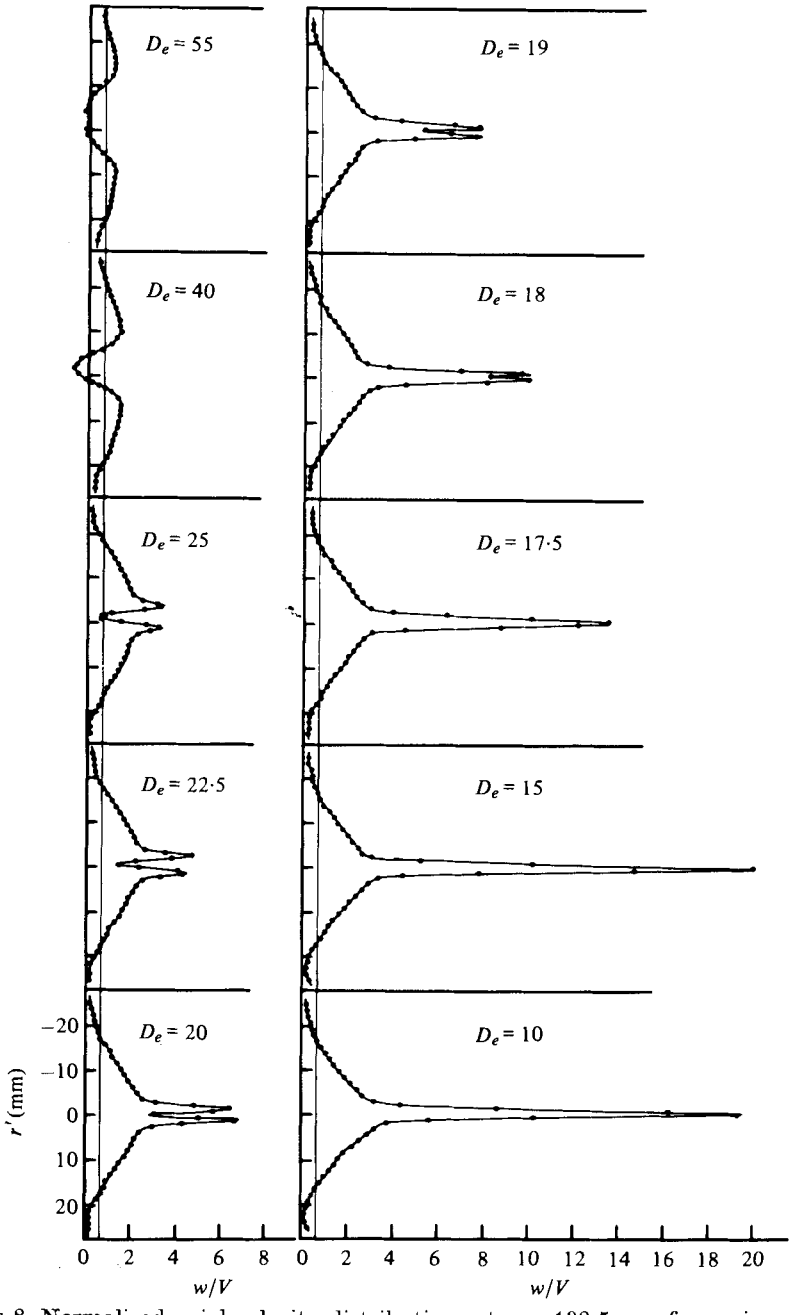

FIGURE 8. Normalized axial-velocity distributions at z = 198·5 mm for various exit diameters.

maximum measured value of $w/V \cong 20$ for $D_e = 15$ mm. The apparently exhaustive study of similarity solutions by Donaldson & Sullivan (1960) contains no hint of the jet-like behaviour for the radial-inflow situation. Although the end-wall boundary layer also exerts a strong influence on the flow, as is clearly seen in figure 7 for profiles measured near the end wall, the measurements indicate that this is not the case through-

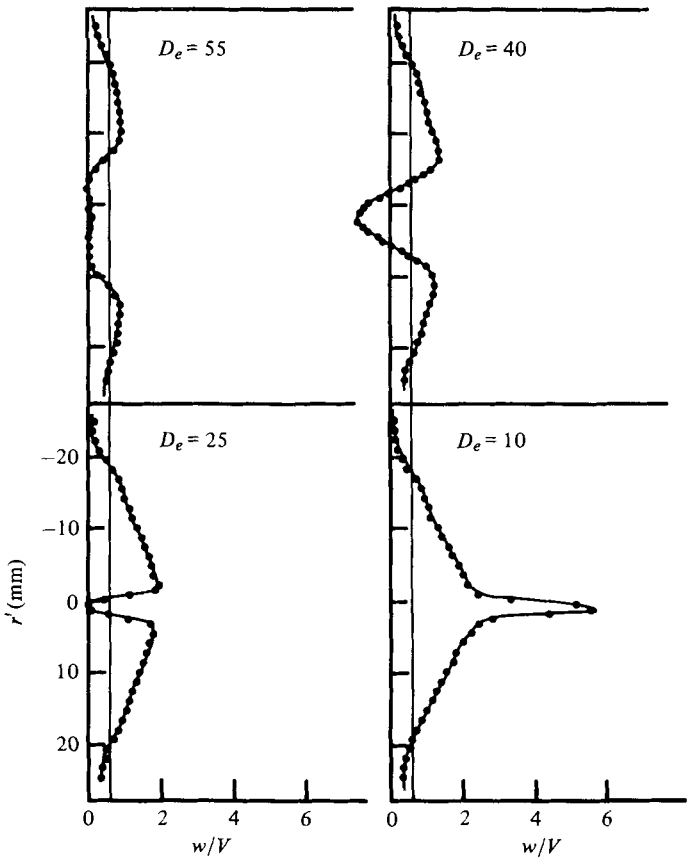

FIGURE 9. Normalized axial-velocity distributions at $z = 193{\cdot}5$ mm for a vortex tube with no central divider.

out the entire flow field. Rather, it is the changes induced in the flow by the exit contraction which seem to be the dominant influence. This point is confirmed by the axial-velocity profiles in figure 9 for the tube with no divider, which show a behaviour pattern similar to that seen in figure 8. For these flows, however, there is no end-wall boundary layer. The reduced peak velocities compared with those in figure 8 for otherwise similar conditions are attributed to the fact that no adjustment was made for the angle ω (all measurements were for 45°) and to the asymmetry in flow mentioned earlier.

Swirl-velocity distributions for $D_e = 10, 18, 25, 40$ and 55 mm are shown in figure 10, again for the tube with the divider installed. In each case data from various axial locations have been plotted on the same axes to emphasize the strong similarity exhibited. Also shown, both superimposed on the data and also for clarity alongside, are curves representing Burgers' (1948) solution, appropriate values for the 'constants' Γ and α/ϵ being chosen by performing a least-squares fit. In view of the significant departure of the axial velocity from the uniform distribution appropriate to Burgers' solution, the degree of agreement with the swirl-velocity measurements is remarkable. The systematic deviations of data near the positions of maximum swirl are attributed to inadequate resolution of the LDA system in this region, and that near the tube walls to the influence of the inflow.

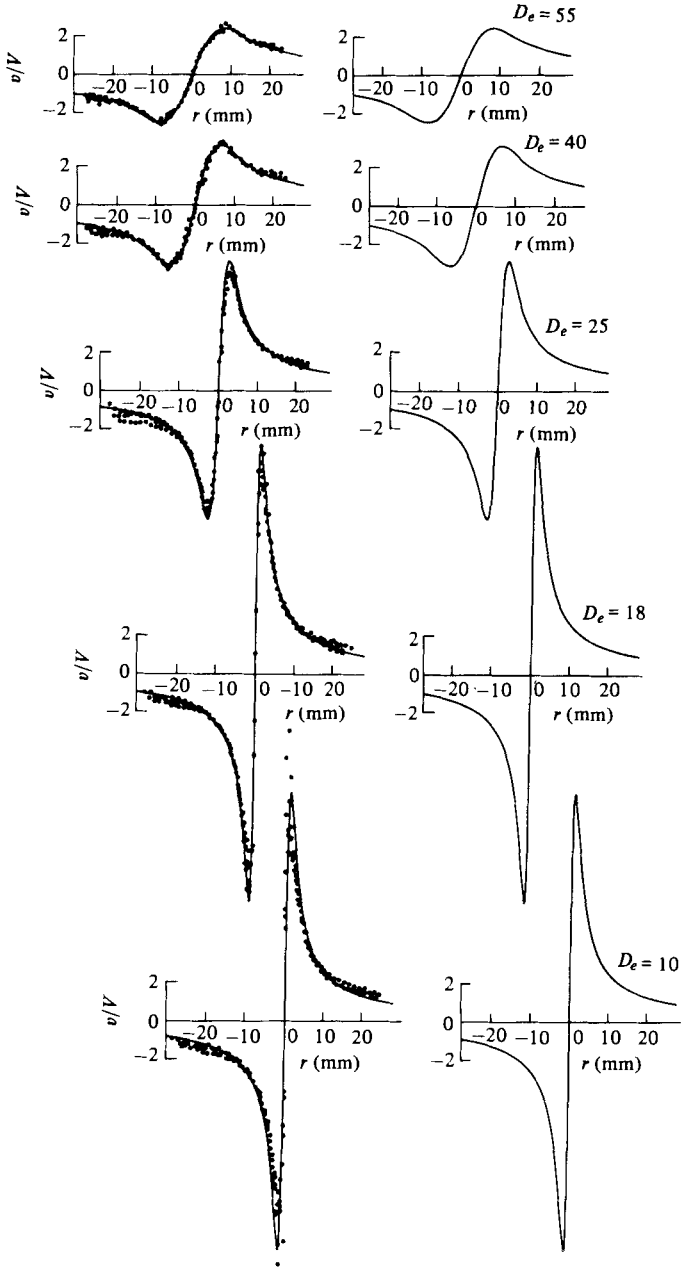

FIGURE 10. Normalized swirl-velocity distributions together with Burgers' analytical solution.

For the swirl too the strong influence of D_e is apparent, not withstanding the remark of Keynes (1960) to the contrary, the maximum swirl velocity v_{max} being increased by an order of magnitude by the reduction of D_e from 55 mm to 10 mm. Since the outer region has a velocity distribution close to that of a potential vortex with $\Gamma/\pi DV \cong 1$, this change in v_{max} is closely associated with a corresponding reduction in core diameter d, as was also revealed by flow visualization.

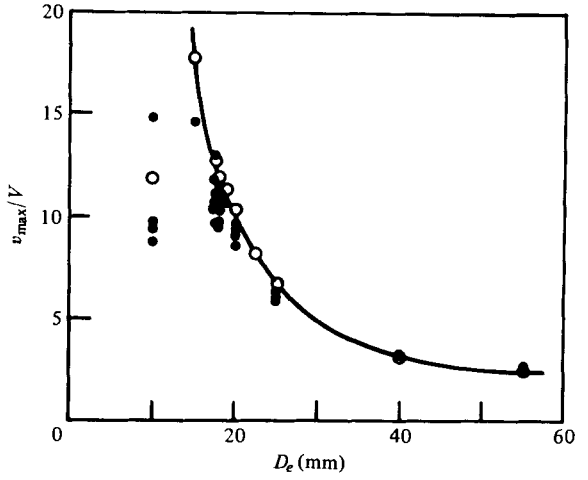

FIGURE 11. Variation of maximum swirl velocity with exit diameter. ●, measured values; ○, from Burgers' average profile.

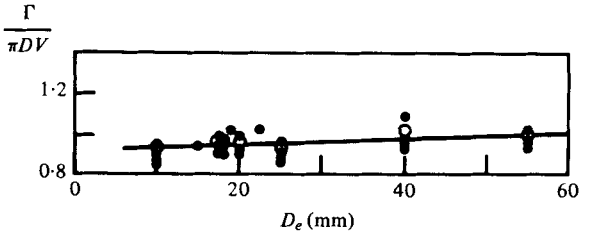

FIGURE 12. Circulation as a function of exit diameter. ●, values for individual profiles; ○, average values.

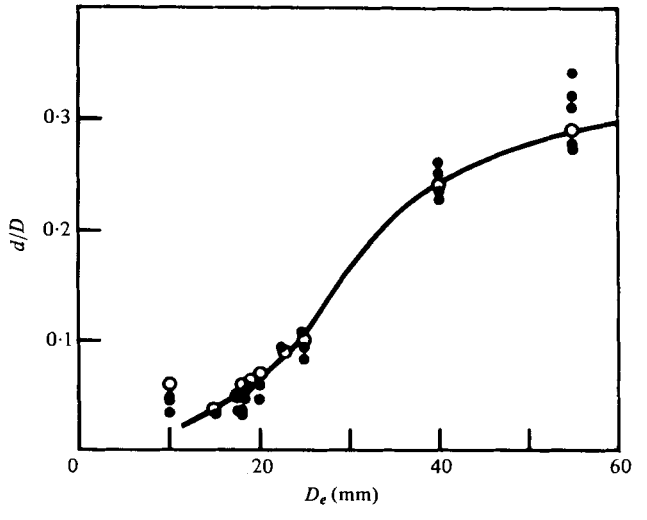

FIGURE 13. Vortex core diameter as a function of exit diameter. Symbols as for figure 11.

As was remarked earlier, the theoretical analysis of vortex flows is difficult and much remains to be done if even their quantitative behaviour is to be adequately described. Figures 11–13 show the variations of some quantities of interest in this respect which have been derived from the LDA measurements. First, in figure 11, data for the maximum swirl velocity are plotted against the exit diameter D_e. The solid points represent directly-measured values, whereas the open circles, through which a curve has been drawn, were obtained from the Burgers' profiles of figure 10. Here again, the poor resolution of the LDA in the vicinity of $v_{\max}$ is regarded as the main reason for the measured data falling for the most part significantly below the Burgers' values. Both here and in figure 13 the data for $D_e = 10$ mm do not follow the consistent trends apparent for the other exit diameters.

The data in figure 12 represent the values of the circulation Γ determined from Burgers' profile, again using the least-squares fit criterion, first to individual swirl profiles (solid points), and second to the accumulated data at various axial locations for a given exit diameter (open circles). As remarked above, $\Gamma/\pi DV \cong 1$, as expected in view of the generally excellent match to the data beyond the core region.

The variation of the core diameter d plotted in figure 13 again emphasizes the strong influence of D_e, although this too was to be expected since from Burgers' solution it may be shown that

$$v_{\max} = 0{\cdot}64\frac{\Gamma}{\pi D}\left(\frac{\alpha D^2}{16\epsilon}\right)^{\frac{1}{2}}, \quad \frac{d}{D} = 1{\cdot}12\left(\frac{\alpha D^2}{16\epsilon}\right)^{-\frac{1}{2}}.$$

The data points have the same significance as in figure 11.

5. Concluding remarks

The LDA measurements presented here reveal the strong influence of the physical boundary conditions on the structure of a confined turbulent vortex. These data exhibit significant departures from existing theoretical descriptions of confined-vortex flow, especially the annular jet-like character adopted by the axial velocity distribution for small exit diameters. The work described is being continued and an extensive series of experiments is now underway in air and water which will include measurements and observations of the flow within and beyond the exit tube, for an undivided tube (free of the effects of the end-wall boundary layer) and for various combinations of tube length L, inlet-slit width t, and exit diameter D_e.

The main parts of the vortex-tube model were machined and assembled by Mr E. Vogt and preliminary LDA measurements carried out by Mr A. Biland. The authors also acknowledge with gratitude the work of Mr L. Hlavac in preparing the colour photographs.

REFERENCES

BAKER, G. R., BARKER, S. J., BOFAH, K. K. & SAFFMAN, P. G. 1974 Laser anemometer measurements of trailing vortices in water. *J. Fluid Mech.* **65**, 325.

BINNIE, A. M. & TEARE, J. D. 1956 Experiments on the flow of swirling water through a pressure nozzle and an open trumpet. *Proc. Roy. Soc.* A **235**, 78.

BÖDEWADT, U. T. 1940 Die Drehströmung über festem Grunde. *Z. angew. Math. Mech.* **20**, 241.

BURGERS, J. M. 1948 A mathematical model illustrating the theory of turbulence. *Adv. Appl. Mech.* **1**, 198.

CASSIDY, J. J. & FALVEY, H. T. 1970 Observations of unsteady flow arising after vortex breakdown. *J. Fluid Mech.* **41**, 727.

CHANAUD, R. C. 1965 Observations of oscillatory motion in certain swirling flows. *J. Fluid Mech.* **21**, 111.

DONALDSON, C. DU P. & SNEDEKER, R. S. 1962 Experimental investigation of the structure of vortices in simple cylindrical vortex chambers. *Aero. Res. Ass. of Princeton, Inc. Rep.* no. 47.

DONALDSON, C. DU P. & SULLIVAN, R. D. 1960 Behaviour of solutions of the Navier–Stokes equations for a complete class of three-dimensional viscous vortices. *Proc.* 1960 *Heat Transfer and Fluid Mech. Inst.*, p. 16. Stanford University Press.

ESCUDIER, M. P. 1979 Estimation of pressure loss in ring-type exit chambers. *Trans. A.S.M.E.* I, *J. Fluids Engng* **101**, 511.

ESCUDIER, M. P. & MERKLI, P. 1979 Observations of the oscillatory behaviour of a confined ring vortex. *A.I.A.A. J.* **17**, 253.

FALER, J. H. 1976 Some experiments in swirling flows: detailed velocity measurements of a vortex breakdown using a laser Doppler anemometer. *N.A.S.A. Contractor Rep.* no. 135115.

FALER, J. H. & LEIBOVICH, S. 1977 Disrupted states of vortex flow and vortex breakdown. *Phys. Fluids* **20**, 1385.

FALER, J. H. & LEIBOVICH, S. 1978 An experimental map of the internal structure of a vortex breakdown. *J. Fluid Mech.* **86**, 313.

HOLMAN, J. P. & MOORE, G. D. 1961 An experimental study of vortex chamber flow. *Trans. A.S.M.E.* D, *J. Basic Engng* **83**, 632.

ITEN, P. D. & DÄNDLIKER, R. 1972 A sampling wide-band demodulator useful for laser Doppler velocimeters. *Proc. I.E.E.E.* **60**, 1470.

KELLER, J. J. & ESCUDIER, M. P. 1980 Theory and observations of waves on hollow-core vortices. *J. Fluid Mech.* (to appear).

KEYNES, J. J. 1960 An experimental study of gas dynamics in high velocity vortex flow. *Proc.* 1960 *Heat Transfer and Fluid Mech. Inst.*, p. 31. Stanford University Press.

LEWELLEN, W. S. 1971 A review of confined vortex flows. *N.A.S.A. Contractor Rep.* no. 1772.

MERKLI, P. & ESCUDIER, M. P. 1979 Observations of flow in a ring inlet chamber. *Trans. A.S.M.E.* I, *J. Fluids Engng* **101**, 135.

NUTTALL, J. B. 1953 Axial flow in a vortex. *Nature* **172**, 582.

ORLOFF, K. L. 1974 Trailing vortex wind-tunnel diagnostics with a laser velocimeter. *A.I.A.A. J. Aircraft* **11**, 477.

ORLOFF, K. L. & BOSSEL, H. H. 1973 Laser Doppler velocity measurements of swirling flows with upstream influence. *N.A.S.A. Contractor Rep.* no. 2284.

SULLIVAN, R. D. 1959 A two-cell vortex solution of the Navier–Stokes equations. *J. Aero. Space Sci.* **26**, 767.

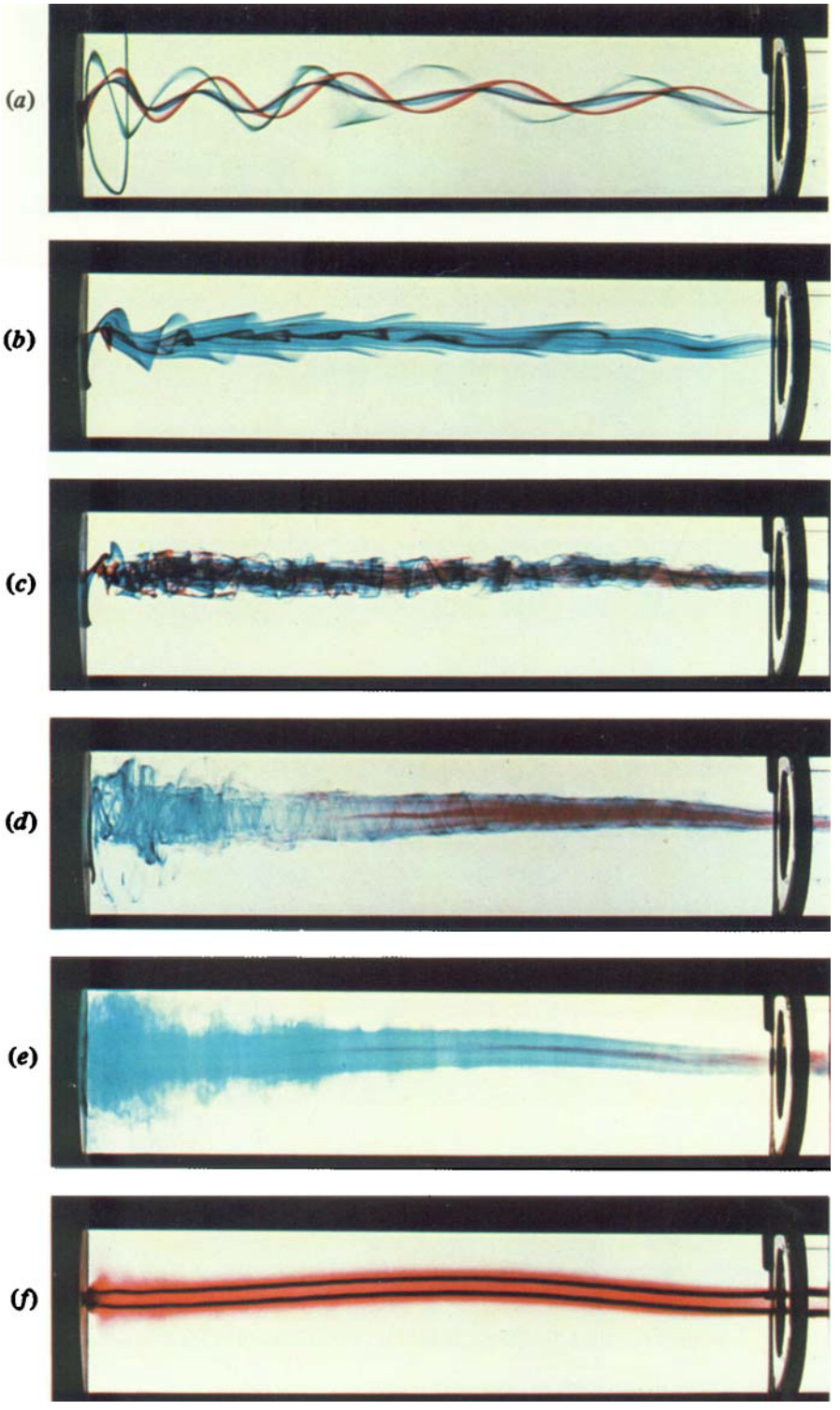

FIGURE 2. Flow visualization photographs of flow in the vortex tube for $D_e = 25$ mm. Flow rates ($l\,s^{-1}$): (*a*) 0·0135; (*b*) 0·0244; (*c*) 0·040; (*d*) 0·10; (*e*) 0·40; (*f*) 3·02.

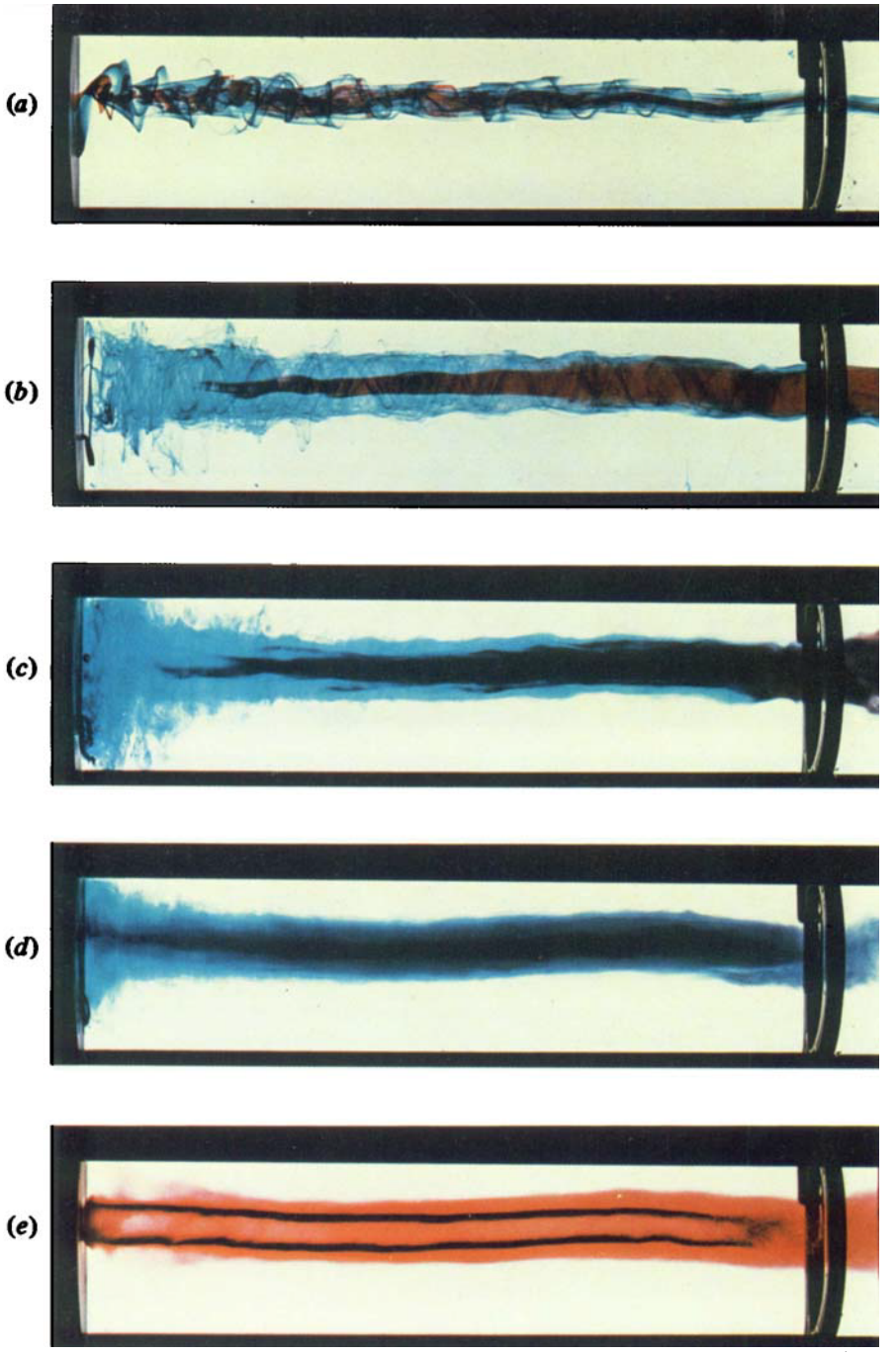

FIGURE 3. Flow visualization photographs of flow in the vortex tube for D_e = 40 mm. Flow rates ($l\,s^{-1}$): (*a*) 0·037; (*b*) 0·104; (*c*) 0·40; (*d*) 0·80; (*e*) 4·7.

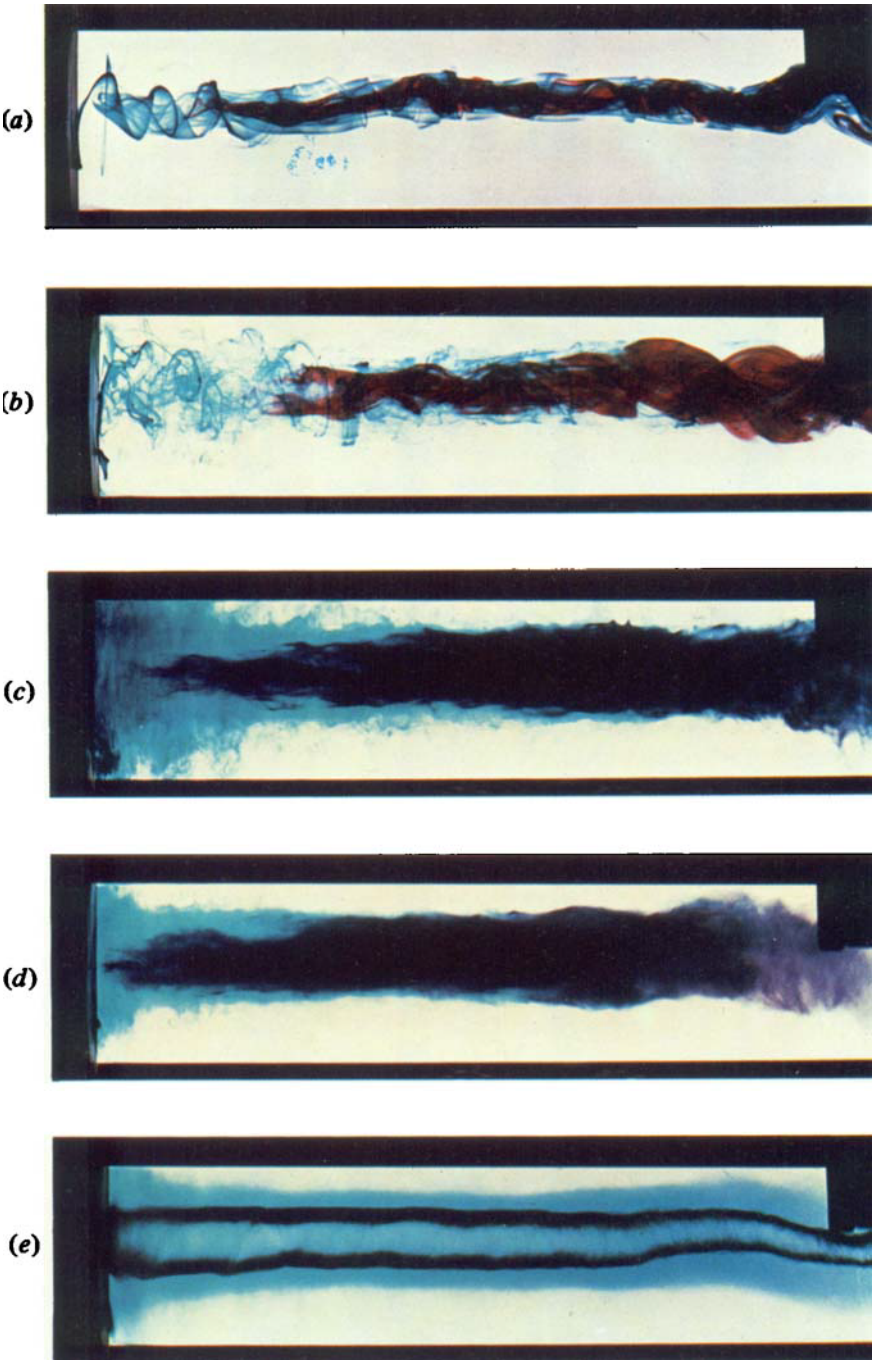

FIGURE 4. Flow visualization photographs of flow in the vortex tube for D_e = 55 mm. Flow rates ($l\,s^{-1}$): (*a*) 0·039; (*b*) 0·098; (*c*) 0·39; (*d*) 0·79; (*e*) 5·7.

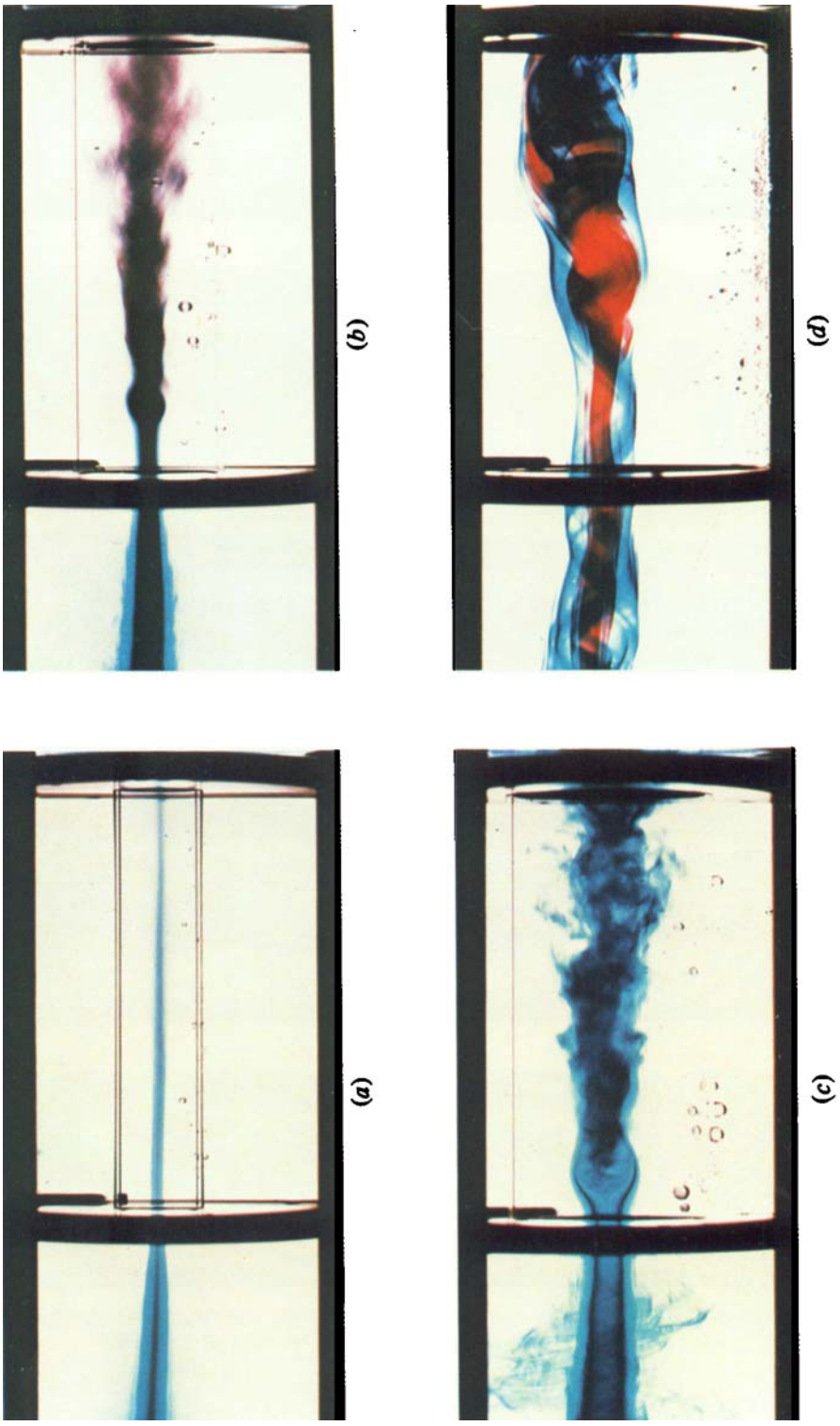

FIGURE 5. Flow visualization photographs of flow in the outlet contractions: (*a*) $D_e = 10$ mm, $Q = 0{\cdot}67\ \mathrm{l\,s^{-1}}$; (*b*) $D_e = 18$ mm, $Q = 0{\cdot}34\ \mathrm{l\,s^{-1}}$; (*c*) $D_e = 25$ mm, $Q = 0{\cdot}136\ \mathrm{l\,s^{-1}}$; (*d*) $D_e = 40$ mm, $Q = 0{\cdot}043\ \mathrm{l\,s^{-1}}$.